Magnetic interactions in α-$NaMnO_2$: Quantum spin-2 system on a spatially anisotropic two-dimensional triangular lattice

Andrej Zorko,* Samir El Shawish, and Denis Arčon
Jožef Stefan Institute, Jamova 39, 1000 Ljubljana, Slovenia

Zvonko Jagličić
Institute of Mathematics, Physics and Mechanics, Jadranska 19, 1000 Ljubljana, Slovenia

Alexandros Lappas
Institute of Electronic Structure and Laser, Foundation for Research and Technology-Hellas, Vassilika Vouton, 71110 Heraklion, Greece

Hans van Tol and Louis Claude Brunel
National High Magnetic Field Laboratory, Florida State University, Tallahassee, Florida 32310, USA
(Received 1 October 2007; revised manuscript received 10 November 2007; published 11 January 2008)

The dc magnetization and the electron spin resonance (ESR) measurements have been performed on α-$NaMnO_2$ polycrystalline sample, a quantum spin system on a frustrated two-dimensional (2D) triangular lattice with spatially anisotropic Heisenberg exchange. The former measurements reveal a realization of the high-spin state ($S=2$) on magnetic Mn^{3+} sites. From the susceptibility curve, we have determined the nearest-neighbor antiferromagnetic exchange coupling constants (namely, in the preferably coupled spin chains, $J_1/k_B=65$ K, and perpendicular to them, $J_2/J_1=0.44$) by employing the finite-temperature Lanczos method. The dominant magnetic anisotropy term of the single-ion type, $D/k_B=-4.1$ K, which establishes an easy-axis direction, is evaluated from the ESR linewidth. We find that the temperature dependence of the linewidth reflects the onset of short-range static spin correlations below room temperature.

DOI: 10.1103/PhysRevB.77.024412 PACS number(s): 75.10.Dg, 75.40.Mg, 76.30.−v

I. INTRODUCTION

Since Anderson's conjecture of a resonating-valence-bond ground state of a two-dimensional (2D) triangular Heisenberg antiferromagnet,[1] extensive research has been carried out on this and related lattices. The emphasis has mainly been put on resolving the issue of whether the interplay between quantum fluctuations and a geometrical frustration can lead to novel magnetic ground states. A predominance of the numerical studies speak in favor of a zero-temperature noncollinear long-range magnetic order on a 2D spin-1/2 triangular lattice, when only isotropic nearest-neighbor (nn) antiferromagnetic exchange is considered.[2–5] When spatially anisotropic exchange interactions are present—exchange coupling between spins along one of the triangle directions (the chains) is different than along the other two directions—the ground-state phase diagram becomes considerably richer. Namely, depending on the ratio between the intrachain J_1 and the interchain coupling J_2, long-range magnetic order on two or three sublattices, incommensurate magnetic order, or various spin-liquid phases can be realized.[5,6] The latter are found in parameter regions where quantum fluctuations are largest, i.e., at $J_1/J_2=0.5$, $J_1/J_2\simeq 0.8$, and $J_1/J_2>4$.[5,7,8] On the other hand, much less is known about the triangular lattice when its sites are occupied by integer spins.

Recently, α-$NaMnO_2$ has been highlighted in this context by Giot *et al.*[9] Its room-temperature crystal structure is of the α-$NaFeO_2$ type, where cubic close packing (*ABCABC*) is realized for oxygen ions. Sodium and manganese ions occupy octahedral sites in consecutive oxygen interlayers,[10] as visualized in Fig. 1(a). The original rhombohedral structure of the iron-based compound is, however, distorted, so that α-$NaMnO_2$ adopts a monoclinic space group ($C2/m$). This is due to the Jahn-Teller (JT) distortion of MnO_6 octahedra that occurs for Mn^{3+} ions ($t_{2g}^3 e_g^1$), in effect lifting the orbital degeneracy. The result is a large difference between apical and equatorial Mn-O distances, 2.40–1.93 Å.[9] According to density functional calculations for the isostructural system α-$LiMnO_2$, JT distortion should lower one of the e_g states below the Fermi level and thus stabilize the high-spin state ($S=2$) on Mn^{3+} sites.[11]

Although the crystal structure of α-$NaMnO_2$ has been known for a rather long time, only a few experimental magnetic characterization attempts were reported in literature, all of them dating more than three decades ago.[10,12] On the contrary, the magnetism of the isostructural α-$LiMnO_2$ has been a subject of extensive research in recent years, mostly due to its favorable characteristics for lithium rechargeable batteries.[13] Recent neutron diffraction investigation of the α-$NaMnO_2$ has suggested that the corresponding spin system, which can be mapped on a spatially anisotropic 2D triangular lattice (see Fig. 1), exhibits 2D antiferromagnetic spin correlations below at least 200 K, which evolve into a three-dimensional (3D) long-range order below $T_N=45$ K.[9] Interestingly enough, below T_N, the magnetic Bragg peaks were found to coexist with Warren-type of scattering, suggesting the coexistence of 3D and 2D magnetic domains. Moreover, the phase transition seems to be of a magnetoelastic type, where the onset of long-range magnetic order is accompanied by structural phase deformation, lowering the symmetry from monoclinic to triclinic.[9]

In order to understand the intriguing magnetic behavior of α-$NaMnO_2$, it is of utmost importance to determine the mag-

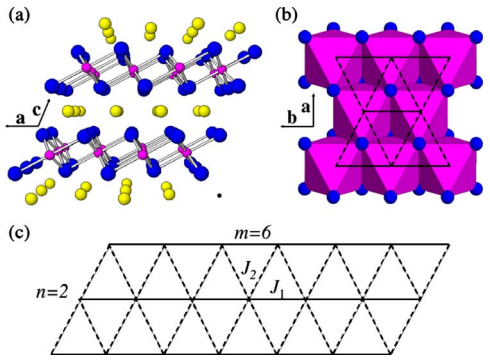

FIG. 1. (Color online) (a) Crystal structure of monoclinic α-$NaMnO_2$ as viewed along the (010) direction. The purple (small), yellow (medium), and blue (large) spheres denote manganese, sodium, and oxygen ions, respectively. (b) Arrangement of edge-sharing MnO_6 octahedra in the *ab* crystal plane and the associated spatially anisotropic triangular lattice of Mn^{3+} $S=2$ spins. (c) The finite $m\times n$ cluster used in the FTLM calculations (periodic boundary conditions) with intrachain J_1 and interchain J_2 exchange.

netic interactions within the spin system. In this paper, we evaluate the major contributions to the spin Hamiltonian. We tackle this problem by modeling the temperature dependence of bulk magnetic susceptibility and electron spin resonance (ESR) spectra in the paramagnetic phase. Our results include both the intrachain and the interchain nn isotropic exchange, as well as the major magnetic anisotropy term. The latter, magnetocrystalline contribution, is shown to be of the single-ion type and sets a magnetic easy axis for the system.

II. EXPERIMENTAL DETAILS

We have synthesized polycrystalline α-$NaMnO_2$ samples according to the published procedure.[10] X-ray powder diffraction measurements confirmed a high-purity $C2/m$ crystalline phase at room temperature.

Magnetization measurements were conducted on a Quantum Design MPMS-XL-5 superconducting quantum interference device magnetometer, in an external field of 1 kOe, between 2 and 400 K. *X*-band electron spin resonance (ν_L =9.40 GHz) measurements were performed in a temperature range between 5 and 600 K on a Bruker E580 FT/CW spectrometer, equipped with a helium-flow cryostat and a preheated-nitrogen-flow heating system for reaching high temperatures. High-field ESR measurements (ν_L=100–400 GHz) were conducted in a transmission mode on a homebuilt spectrometer with a Gunn-diode source at NHMFL, FL.

III. THEORETICAL BACKGROUND

As imposed by the crystal structure [Fig. 1(a)], the magnetic properties of the presently investigated layered compound should be well accounted for by the spatially anisotropic Heisenberg model on a triangular lattice [Fig. 1(b)]. Due to the large interlayer distance, possible interlayer superexchange pathways include several ions and the interlayer coupling can be neglected at high temperatures. The corresponding 2D spin Hamiltonian in the external magnetic field **H** can then be written as

$$\mathcal{H} = J_1 \sum_{(ij)} \mathbf{S}_i \cdot \mathbf{S}_j + J_2 \sum_{[kl]} \mathbf{S}_k \cdot \mathbf{S}_l - g\mu_B H \sum_i S_i^z + \mathcal{H}', \quad (1)$$

where the first two sums add up to the exchange Hamiltonian $\mathcal{H}_e$, with (ij) as nn intra-chain and $[kl]$ as nn interchain spin pairs. The chain direction corresponds to the crystal *b* axis and the *z* axis has been chosen to be that of the magnetic field *H*. The third sum denotes the Zeeman Hamiltonian $\mathcal{H}_Z$ and the term $\mathcal{H}'$ represents the magnetic anisotropy. For Mn^{3+} ions, the latter is dominantly of the single-ion type, i.e.,

$$\mathcal{H}' = D \sum_i (S_i^\xi)^2 = D \sum_i (S_i^z \cos\theta - S_i^x \sin\theta)^2. \quad (2)$$

Here, the axis ξ, tilted by the angle θ from the *z* axis, denotes the direction of the Jahn-Teller distortion of MnO_6 octahedra in the *ac* crystal plane. Since each intrachain as well as interchain nn Mn–Mn bond features a center of inversion, the Dzyaloshinsky-Moriya antisymmetric exchange interaction is forbidden between nearest neighbors by symmetry.[14] Other contributions, including the symmetric part of the anisotropic exchange and the dipolar interaction, are not important, as further argued in Sec. V.

In the case of a large isotropic exchange compared to other interactions in the Hamiltonian in Eq. (1), the ESR spectra exhibit a Lorentzian line shape.[15] For broad lines (of the order of the resonance field H_{res}), both circular polarizations of the microwave irradiation, determining the resonances at $\pm H_{res}$, have to be taken into account,

$$\frac{dI}{dH} \propto \frac{d}{dH}\left(\frac{\Delta H + 2r(H - H_{res})}{4(H - H_{res})^2 + \Delta H^2} + \frac{\Delta H + 2r(H + H_{res})}{4(H + H_{res})^2 + \Delta H^2}\right). \quad (3)$$

In this expression, the parameter ΔH denotes a linewidth, while *r* represents the amount of a dispersion admixed into an absorption spectrum. In insulating materials, one usually encounters pure absorption Lorentzian lines (r=0). However, asymmetric dispersive Lorentzians, i.e., Dysonian-like line shapes, can be observed if the dispersion contribution is admixed with the absorption. This is in general expected if the magnetic anisotropy of a particular system results in very broad ESR lines (of the order of H_{res}) due to nondiagonal terms of a susceptibility tensor.[16] Alternatively, Dysonian line shapes are in general observed in metallic samples due to a skin effect.[17]

At high temperatures ($k_BT \gg g\mu_BH$), the ESR linewidth can be approximated by[18]

$$\Delta H = C \frac{k_B}{g\mu_B} \sqrt{\frac{M_2^3}{M_4}}, \quad (4)$$

where the second and the fourth moment of the absorption spectra have the following form:

$$M_2 = \frac{\langle [\mathcal{H}', S^+][S^-, \mathcal{H}'] \rangle}{\langle S^+ S^- \rangle}, \quad (5)$$

$$M_4 = \frac{\langle [\mathcal{H} - \mathcal{H}_Z, [\mathcal{H}', S^+]][\mathcal{H} - \mathcal{H}_Z, [\mathcal{H}', S^-]] \rangle}{\langle S^+ S^- \rangle}, \qquad (6)$$

respectively. In the above expressions, $[\cdots]$ denotes commutators while $\langle \cdots \rangle$ stands for thermal averaging.

The constant C depends on the approximation of the line shape.[18] The moments of a purely Lorentzian line diverge while the theoretical ones, determined by the spin Hamiltonian, are finite. Consequently, the measured ESR lines are Lorentzian within a certain field range around H_{res} and decay faster in their extreme wings.[19] Therefore, such approximations have a physical footing. One should use the approximation line shape for which the agreement between the theoretical exchange field $H_{ex}=k_B/g\mu_B\sqrt{M_4/M_2}$, determined by the spin Hamiltonian, and the one given by this line shape is the best. Usually, the approximation where the Lorentzian line in multiplied with the broad Gaussian $G(H) \propto \exp[-(H-H_{res})^2/2H_{ex}^2]$ is applicable to systems with strong exchange, assuming that the decay of spin correlations is Gaussian in time.[19] In this case, $C=\sqrt{2\pi}$. Lastly, it should be stressed that a temperature dependent linewidth reflects the evolution of the spin correlation functions through Eqs. (4)–(6).[15]

For the spin Hamiltonian considered in Eq. (1), the moments can be calculated exactly in the infinite-temperature limit, when spin-spin correlations at different sites become negligible; $M_2=\frac{21}{10}D^2(1+\cos^2\theta)$ and $M_4=\frac{252}{5}D^2(J_1^2+2J_2^2)(1+\cos^2\theta)$, where only the leading term in magnetic anisotropy is retained for M_4. Inserting these expressions into Eq. (4) and performing powder averaging, we derive the following ESR linewidth expression:

$$\Delta H_\infty = \frac{7\sqrt{3\pi}}{15}\frac{k_B}{g\mu_B}\frac{D^2}{\sqrt{J_1^2+2J_2^2}}. \qquad (7)$$

In addition to the above exact expressions, we have carried out quantitative analysis based on numerical calculations of the uniform susceptibility $\chi_0 \propto \langle S^{z2}\rangle/NT$ and static spin correlations in Eqs. (4)–(6) of finite N-site spin clusters. These calculations were carried out by means of the finite-temperature Lanczos method (FTLM).[20] The FTLM is nonperturbative, based on the Lanczos procedure of exact diagonalization and random sampling over initial wave functions. It is particularly convenient for triangular lattices as it does not suffer from the minus-sign problem, which may arise in, e.g., quantum Monte Carlo simulations on such geometrically frustrated systems. Moreover, the FTLM continuously connects the high- and low-temperature regimes and incorporates as well as takes advantage of the symmetries of the problem. We have considered the translational symmetry and the total S^z invariance of the Hamiltonian in Eq. (1) for $\theta=0$. In this way, we managed to compute clusters with up to $N=12$ spin-2 sites. Among the shortcomings of the FTLM is its limitation in reaching arbitrary low temperatures on finite systems, which leads to the appearance of sizable finite-size effects. We have analyzed the convergence of the method by applying FTLM to various $N=m\times n$ clusters defined in Fig. 1(c) using periodic boundary conditions [see Fig. 2(b)]. From this finite-size analysis, we safely conclude that an $N=6\times 2$ cluster provides a good thermodynamic limit, where the estimated error of the calculated susceptibility is less than 5% in a given temperature range.

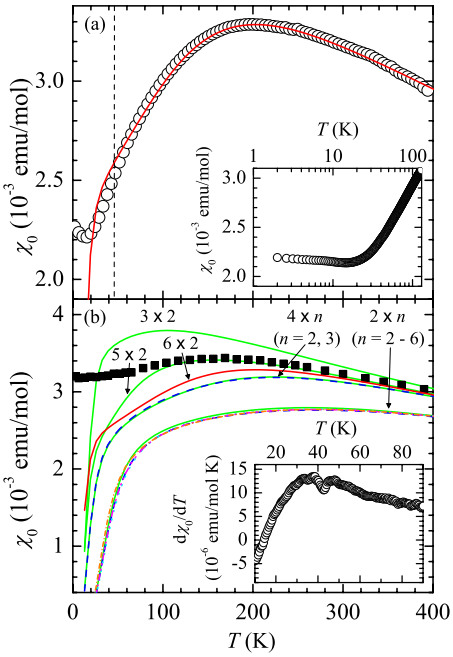

FIG. 2. (Color online) (a) The temperature dependence of the magnetic susceptibility ($\chi_0=M/H$) measured at 1 kOe (circles) and the corresponding numerical fit on $N=6\times 2$ site cluster (solid line) determining the magnetic exchange parameters, $J_1/k_B=65$ K and $J_2/k_B=29$ K. The fit corresponds to temperatures above $T_N=45$ K, which is emphasized with the vertical line. The inset shows the low-temperature part. (b) The finite-size analysis of the susceptibility calculated by FTLM on various $N=m\times n$ clusters, with $m=2-6$ and $N\leqslant 12$ (lines). We also show a classical Monte Carlo result on 16×16 site cluster (squares) to emphasize the quantum effects in a given spin-2 system. All curves are calculated with the same exchange parameters as in (a). The inset shows the temperature derivative of the measured susceptibility.

IV. EXPERIMENTAL RESULTS

A. dc susceptibility

The magnetic susceptibility of the sample, i.e., magnetization divided by the applied magnetic field of 1 kOe, is shown in Fig. 2 (we note that the notation $\chi_0=M/H$ is valid only in the paramagnetic phase). It exhibits a broad maximum around 200 K, characteristic of spin correlations building up in low-dimensional antiferromagnets. This feature was recently thoroughly investigated for spin-1/2 spatially anisotropic triangular lattices via high-temperature series-expansion calculations.[21]

The broad maximum of the susceptibility curve suggests a large negative Curie-Weiss temperature. To accurately determine this parameter, the susceptibility curve should be measured to much higher temperatures, since it will get greatly overestimated if the estimate is done at temperatures of the order of or below the Curie-Weiss temperature.[21] On the

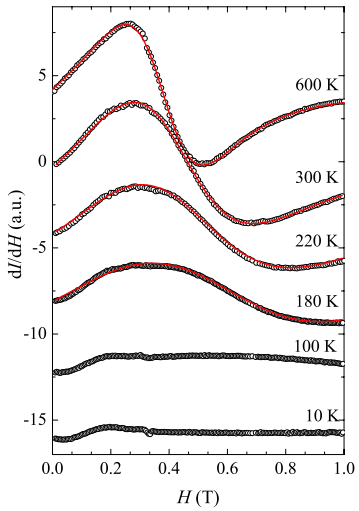

FIG. 3. (Color online) The temperature evolution of the derivative *X*-band ESR spectra in α-$NaMnO_2$ (circles) and the corresponding fits (solid lines), given by Eq. (3).

other hand, its sign, speaking in favor of antiferromagnetic correlations, is enough to determine the spin state of the Mn^{3+} magnetic moments in α-$NaMnO_2$. Namely, the antiferromagnetic correlations reduce the susceptibility below the value given by the Curie law at each temperature in the investigated temperature interval. Since only $S=2$ spins yield a value given by the Curie law, $C/T=7.5\times10^{-3}$ emu/mol, which is above the measured susceptibility at 300 K, $\chi_0(300\ \mathrm{K})=3.1\times10^{-3}$ emu/mol, this confirms the realization of the high-spin state. We stress at this point that the realization of such state is in accordance with density functional calculations for the isostructural α-$LiMnO_2$.[11]

Below 20 K, the magnetization exhibits a distinctively different behavior. Namely, at around 20 K, it shows a broad minimum and then starts to slowly increase with decreasing temperature. It must be stressed that this increase is much slower than the one described by the Curie law [see inset to Fig. 2(a)], as expected in the case of paramagnetic impurities. The plateaulike dependence should therefore be an intrinsic property.

The change of the behavior at low temperatures can be attributed to the long-range magnetic ordering, taking place below $T_N=45$ K. The ordering is evidenced by the presence of magnetic Bragg peaks in the neutron diffraction patterns.[9] In dc magnetization measurements, it is indicated by a subtle "kink," clearly recognized only on a $d\chi/dT$ plot [inset to Fig. 2(b)]. Similar subtle changes were, for instance, observed in the susceptibility curve of the orthorhombic $LiMnO_2$ at the long-range magnetic-ordering temperature.[22]

B. Electron spin resonance

The *X*-band ($\nu=9.40$ GHz) ESR spectra are very broad (Fig. 3). The linewidth increases monotonically with decreasing temperature, which makes the spectra unobservably broad below around 180 K. The temperature evolution of the linewidth, shown in Fig. 4, was determined by fitting the

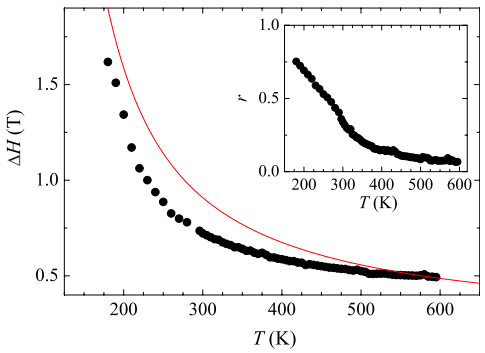

FIG. 4. (Color online) The experimental (circles) and numerically predicted (line) temperature dependence of the ESR linewidth in α-$NaMnO_2$ at 9.40 GHz. The FTLM calculation was performed on $N=6\times2$ site cluster with the same exchange parameters as in Fig. 2(a) and $|D|/k_B=4.1$ K. The inset shows the temperature changes in the dispersion-to-absorption ratio.

experimental spectra to Eq. (3). At high temperatures, the width approaches a constant value, suggesting that *static* spin correlations are diminishing. It is worth noting that no sudden changes in the temperature dependence of the linewidth are observed. The Jahn-Teller distortion, which is the main source of the magnetic anisotropy in the system, should therefore remain static on the ESR timescale at least up to 600 K.

The observed ESR spectra are of the Dysonian shape, marking the admixture of the dispersion and the absorption signal. As they broaden with decreasing temperature, the Dysonian character is progressively enhanced. The increase of the dispersion-to-absorption ratio parameter *r* with decreasing temperature is shown in the inset to Fig. 4. Similar behavior[23] was recently observed in the insulating quasi-2D compound GdI_2. A qualitative explanation, based on the effects of the anisotropic susceptibility on the line shape, reveals that the admixture of the dispersion is enhanced with the line broadening and/or the line shift.[16] This picture is applicable to α-$NaMnO_2$ since recent density-of-states and band-structure calculations confirmed that the compound is semiconducting.[24] Alternatively, increased conductivity with decreasing temperature could potentially lead to the observed line shape transformation.[17]

We have performed further ESR measurements at frequencies between 100 and 400 GHz in a transmission setup. Since the admixture of the dispersion and the absorption mode is intrinsic in these measurements, no further conclusion can be drawn on the line shape. The ESR spectra remain single-line Dysonian (Fig. 5); however, they exhibit some frequency broadening, as shown in Fig. 6(a). The nonmodified line shape infers that this broadening is not due to *g*-factor anisotropy. Also, *g*-strain effects are highly unlikely, since *g*-factor distribution with a width of $\delta g\approx0.1$ would be needed. Therefore, the frequency broadening at room temperature may be reflecting the development of spin correlations.

Since at higher frequencies the room-temperature linewidth becomes small compared to the resonance field, these measurements can be utilized for a more accurate determina-

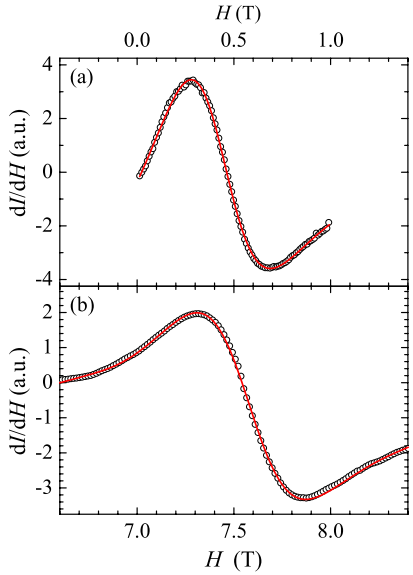

FIG. 5. (Color online) The room-temperature derivative ESR spectrum of α-$NaMnO_2$ measured at (a) 9.40 GHz and (b) 211.2 GHz. The solid lines are Lorentzian fits [Eq. (3)].

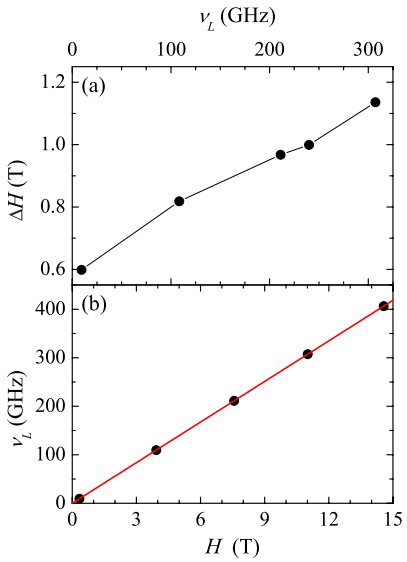

FIG. 6. (Color online) (a) The room-temperature frequency dependence of the linewidth and (b) the frequency-field dependence, determining the g factor $g=1.993$.

tion of the powder-averaged g factor. The straight line in Fig. 6(b) corresponds to $g=1.993$. Such value, slightly below the free electron value $g_0=2.0023$, is commonly observed for less than half-filled d-orbital transition metals, providing that an orbital singlet is present.[25]

V. DISCUSSION

The parameters of the exchange Hamiltonian in Eq. (1) are readily obtained by fitting χ_0, calculated by FTLM, to the measured data M/H above T_N, as shown in Fig. 2(a). The optimal parameters for the $N=6\times2$ site cluster are $J_1/k_B=65\pm1$ K and $J_2/k_B=29\pm1$ K, which yield the exchange ratio $J_2/J_1=0.44$. In this particular calculation, we neglected the magnetic anisotropy term $\mathcal{H}'$, which only contributes at temperatures below $T\sim D$.

Since the parameters are obtained on a rather small system of $N=12$ spins (due to the limitation set by the spin size), we also show the convergence of the calculated $\chi_0(T)$ for various clusters of size $N=m\times n$ [Fig. 1(c)]. The FTLM lines, shown in Fig. 2(b), exhibit a rapid convergence for a fixed m and a varying n and a slower convergence, in an alternating odd and even manner, for a fixed n and a varying m. Although the thermodynamic limit is not perfectly reached for $N=6\times2$, we can estimate the finite-size error of the calculated susceptibility by comparing the optimal parameters on all 12-site clusters. The error is below 5% for all $T>T_N$.

The above-evaluated exchange parameters reveal that the intrachain exchange is dominant in α-$NaMnO_2$. In the case of the isostructural α-$LiMnO_2$, recent local-spin-density approximation calculations predicted that the intrachain exchange should be about three times stronger than the interchain exchange and that the interlayer coupling is significantly weaker.[26] These predictions are in good agreement with our results for the α-$NaMnO_2$.

The exchange coupling constants deduced from our numerical analysis correspond to the high-temperature monoclinic phase. The crystal structure undergoes a triclinic distortion below the Néel-ordering transition.[9] As a result, one of the interchain Mn-Mn distances is lengthened and the other is shortened. These changes are marginal, i.e., of the order of 0.1%; therefore, the magnetic exchange constants should not change drastically at the structural phase transition. It is important to note though that the triclinic distortion lifts the frustration of the interchain coupling J_2 and thus helps in stabilizing the long-range magnetic order, as pointed out by Giot *et al.*[9] We foresee that magnetic anisotropy can be another key factor because it sets a magnetic easy-axis direction and thus stabilizes 3D magnetic ordering. It is evaluated from the present ESR results in the following paragraphs.

The recorded ESR spectra can be assigned to Mn^{3+} magnetic moments in the high-spin $S=2$ state. For instance, similar enhanced ESR linewidths were observed in $La_{1-x}Sr_xMnO_3$, where it was shown that both Mn^{3+} and Mn^{4+} moments contributed to the observed ESR signal.[27] The ESR response of the 4^+ valence state is commonly observed, as the Mn^{4+} ion features an orbital singlet in an octahedral crystal field. The spin-lattice relaxation rate and magnetic anisotropy are therefore much lower than those for Mn^{3+} ion, where an orbital doublet is present.[25] The Mn^{3+} ESR contribution can, however, be observable if the local environment is Jahn-Teller distorted. Such tetragonal distortion of the crystal field, which suppresses the orbital degeneracy of the Mn^{3+} ions, is present in the investigated compound, as the octahedra are significantly elongated.[9] The observed small g shift (away from g_0) indicates that the strength of the spin-orbit coupling is small compared to the energy separation of the orbital ground state to other orbital states. As a result, the admixture of the excited states in the orbital ground state, induced by the spin-orbit coupling, is marginal.

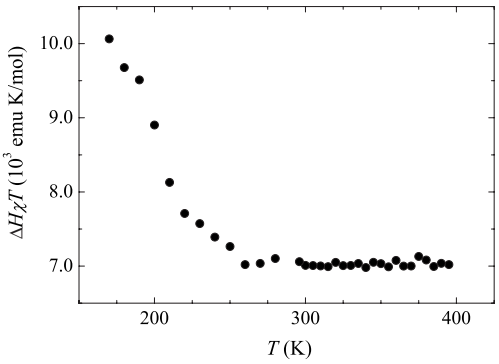

FIG. 7. The temperature dependence of the ESR linewidth (at 9.40 GHz) multiplied by the susceptibility and temperature.

The temperature dependence of the ESR linewidth reflects the evolution of the spin correlations in the investigated system. In order to present this clearly, it is convenient to plot the dependence of $\Delta H\chi T$ versus T, which is constant when static spin correlations are negligible.[28] The temperature evolution of $\Delta H\chi T$ shows a plateaulike behavior down to 260 K and a pronounced increase below this temperature (Fig. 7). This experimental finding is likely to be related to short-range, static spin correlations, developing below the plateau region. Recent neutron diffraction experiments support this picture. Namely, diffusive peaks, emerging as a consequence of 2D antiferromagnetic correlations, are present in the powder diffraction patterns at least up to 200 K.[9]

On the other hand, the constant high-temperature value, $\Delta H\chi T = 7.0 \times 10^3$ emu K/mol, allows one to evaluate the infinite-temperature linewidth, where χT becomes equal to the Curie constant $C = N_A S(S+1) g^2 \mu_B^2 / 3k_B$. Taking $g = 1.993$, we calculate the limiting value of the linewidth $\Delta H_\infty = 0.23$ T. Using Eq. (7), the value of ΔH_∞ and the exchange constants $J_1/k_B = 65$ K and $J_2/k_B = 29$ allow an estimate of the single-ion anisotropy, $|D|/k_B = 4.1$ K.

Single-ion anisotropy of the order of a few Kelvin was also numerically calculated for Mn^{3+} ions in low symmetry environments.[29] We expect that any additional term of the magnetic anisotropy in α-$NaMnO_2$ should be much smaller than the single-ion anisotropy. The magnitude of the latter is of the order of $D \approx \Delta g^a \lambda$, and therefore much larger than the symmetric anisotropic exchange, which is of the order of $(\Delta g/g)^2 J/k_B \approx 6$ mK. This is because the anisotropy of the g shift Δg^a is in general comparable to the shift $\Delta g = g - g_0$ itself, so that $\Delta g^a \gg (\Delta g/g)^2$. On the other hand, the spin-orbit coupling should remain larger than the exchange coupling, even if it is considerably reduced from its free-ion value $\lambda/k_B = 505$ K.[31] Lastly, dipolar interactions are also in the subkelvin range in the investigated system. All these confirm our initial assumption of the anisotropy Hamiltonian in Eq. (2).

The above procedure does not allow one to determine the sign of the single-ion anisotropy, since the linewidth is given by the square of this parameter. However, the sign can be argued by considering the perturbation effect of the spin-orbit coupling on the fivefold spin degenerate orbital ground state of the Mn^{3+} ion in the tetragonally elongated ligand environment. Such environment yields a negative single-ion anisotropy constant.[30] This conceptional argument corresponds well to the experimental results. Namely, the magnetic moments order in the direction of the Jahn-Teller distorted octahedra in the long-range magnetically ordered phase,[9] which proves the presence of a magnetic easy axis rather than a magnetic easy plane.

The temperature evolution of the spin correlations, reflected in the broadening of the ESR spectra with decreasing temperatures, was simulated numerically by FTLM [Eqs. (4)–(6)]. Having the size of the single-ion anisotropy ($|D|/k_B = 4.1$ K) fixed by the high-temperature ESR linewidth limit and the exchange parameters ($J_1/k_B = 65$ K, $J_2/k_B = 29$ K) determined from the susceptibility fit, we are left with no free parameters in the calculation of $\Delta H(T)$. The agreement with the experimental values is shown in Fig. 4.[32] The discrepancy between the theory and the experiment is below 25% at all temperatures. As all the parameters are fixed, this quantitative agreement supports further the relevance of the proposed Hamiltonian and the validity of the extracted physical quantities.

Despite the onset of the long-range magnetic order, α-$NaMnO_2$ can still be regarded as a system featuring strong frustration effects. According to the notation introduced by Ramirez,[33] highly frustrated lattices are characterized by an empirical factor $f = |\Theta_{CW}|/T_c$, with values in excess of 10, where Θ_{CW} represents the Curie-Weiss temperature and T_c a critical temperature corresponding to cooperative magnetic ordering or spin freezing. As our mean-field result yields $\Theta_{CW} = -(2J_1 + 4J_2) S(S+1)/3k_B = -490$ K, with $T_c = T_N = 45$ K from neutron diffraction,[9] the investigated compound appears to be strongly frustrated ($f = 11$). Such a high degree of geometric frustration may point to the importance of quantum fluctuations in the cooperative paramagnetic regime, $T_c \lesssim T \lesssim |\Theta_{CW}|$, of the given spin-2 system. We confirm this in Fig. 2(b) by comparing the optimal $\chi_0(T)$, calculated by FTLM on 6×2 site cluster, with the one simulated with the same parameters on 16×16 site cluster using a classical Monte Carlo (MC) approach.[34] Having in mind that both calculations are close to their thermodynamic limit, a large discrepancy between the curves is observed below room temperature. We wish to stress that the MC calculations cannot satisfactorily explain the downturn of the experimental susceptibility, even when optimizing the parameters for this particular calculations. From the discrepancy between the classical and the quantum approach, we envisage that spin fluctuations, enhanced by strong geometrical frustration, are important even up to room temperature and, hence, a quantum-mechanical description is necessary.

These findings appeal to further experimental studies of the α-$NaMnO_2$ spin system as well as to thorough theoretical investigation of the 2D triangular spin lattice with sizable magnetic anisotropy and higher and/or integer spin values. The former is known to suppress spin fluctuations and integer spins have recently been shown to significantly weaken the frustration effects in nn Heisenberg kagomé lattices.[35]

VI. CONCLUSIONS

In summary, our magnetization and ESR data allow us to evaluate the major contributions to the spin Hamiltonian of

the layered α-$NaMnO_2$ compound. Its Jahn-Teller distorted structure is stable at least up to 600 K and assigns the corresponding spin-2 system on a 2D spatially anisotropic triangular Heisenberg lattice ($J_1/k_B=65$ K, $J_2/J_1=0.44$), with significant easy-axis magnetic anisotropy. This anisotropy of single-ion type, $D/k_B=-4.1$ K, suppresses the spin fluctuations and assists in stabilizing the 3D long-range magnetic order below $T_N=45$ K. The ESR results suggest that the system displays static spin correlations almost up to room temperature.

ACKNOWLEDGMENTS

A.Z. and D.A. acknowledge the financial support of the Slovenian Research Agency for the research projects J1-6516 and Z1-9530-0106-06. Some of the results shown in Fig. 2 have been obtained by using the ALPS libraries.[34]

*andrej.zorko@ijs.si

[1] P. W. Anderson, Mater. Res. Bull. **8**, 153 (1973).
[2] D. A. Huse and V. Elser, Phys. Rev. Lett. **60**, 2531 (1988).
[3] B. Bernu, C. Lhuillier, and L. Pierre, Phys. Rev. Lett. **69**, 2590 (1992).
[4] L. Capriotti, A. E. Trumper, and S. Sorella, Phys. Rev. Lett. **82**, 3899 (1999).
[5] Zheng Weihong, R. H. McKenzie, and R. P. Singh, Phys. Rev. B **59**, 14367 (1999).
[6] S. Yunoki and S. Sorella, Phys. Rev. B **74**, 014408 (2006).
[7] A. E. Trumper, Phys. Rev. B **60**, 2987 (1999).
[8] J. Merino, R. H. McKenzie, J. B. Marston, and C. H. Chung, J. Phys.: Condens. Matter **11**, 2965 (1999).
[9] M. Giot, L. C. Chapon, G. Androulakis, M. A. Green, P. G. Radaelli, and A. Lappas, Phys. Rev. Lett. **99**, 247211 (2007).
[10] J.-P. Parant, R. Olazcuaga, M. Devalette, C. Fouassier, and P. Hagenmuller, J. Solid State Chem. **3**, 1 (1971).
[11] S. K. Mishra and G. Ceder, Phys. Rev. B **59**, 6120 (1999).
[12] Von M. Jansen and R. Hoppe, Z. Anorg. Allg. Chem. **399**, 163 (1973).
[13] A. R. Armstrong and P. G. Bruce, Nature (London) **381**, 499 (1996).
[14] T. Moriya, Phys. Rev. **120**, 91 (1960).
[15] R. Kubo and K. Tomita, J. Phys. Soc. Jpn. **9**, 888 (1954).
[16] H. Benner, M. Brodehl, H. Seitz, and J. Wiese, J. Phys. C **16**, 6011 (1983).
[17] S. E. Barnes, Adv. Phys. **30**, 801 (1981).
[18] T. G. Castner, Jr. and M. S. Seehra, Phys. Rev. B **4**, 38 (1971).
[19] See, for instance, G. E. Pake, *Paramagnetic Resonance* (Benjamin, New York, 1962).
[20] J. Jaklič and P. Prelovšek, Adv. Phys. **49**, 1 (2000); Phys. Rev. Lett. **77**, 892 (1996); Phys. Rev. B **49**, 5065 (1994).
[21] W. Zheng, R. R. P. Singh, R. H. McKenzie, and R. Coldea, Phys. Rev. B **71**, 134422 (2005).
[22] J. E. Greedan and P. N. Raju, J. Solid State Chem. **128**, 209 (1997).
[23] J. Deisenhofer, H.-A. Krug von Nidda, A. Loidl, K. Ahn, R. K. Kremer, and A. Simon, Phys. Rev. B **69**, 104407 (2004).
[24] O. I. Velikokhatnyi, C.-C. Chang, and P. N. Kumta, J. Electrochem. Soc. **150**, A1262 (2003).
[25] A. Abragam and B. Bleaney, *Electron Paramagnetic Resonance of Transition Ions* (Clarendon, Oxford, 1970).
[26] D. J. Singh, Phys. Rev. B **55**, 309 (1997).
[27] V. A. Ivanshin, J. Deisenhofer, H.-A. Krug von Nidda, A. Loidl, A. A. Mukhin, A. M. Balbashov and M. V. Eremin, Phys. Rev. B **61**, 6213 (2000).
[28] D. L. Huber and M. S. Seehra, J. Phys. Chem. Solids **36**, 723 (1975).
[29] A. Bencini, I. Ciofini, and M. G. Uytterhoeven, Inorg. Chim. Acta **274**, 90 (1997).
[30] J.-P. Renard and M. Velazquez, Eur. Phys. J. B **34**, 41 (2003).
[31] J. Bendix, M. Brorson, and C. E. Schäffer, Inorg. Chem. **32**, 2838 (1993).
[32] We note that $\Delta H(\theta) \propto 1+\cos^2\theta$ (see the expressions for M_2 and M_4 in the text), which considerably simplifies the calculation of the powder-averaged ESR linewidth: $\Delta H=2/3\Delta H(\theta=0)$. At $\theta=0$, the total S^z of the Hamiltonian in Eq. (1) is a good quantum number, allowing us to use systems with up to $N=12$ spin-2 sites.
[33] A. P. Ramirez, Annu. Rev. Mater. Sci. **24**, 453 (1994).
[34] F. Alet *et al.*, J. Phys. Soc. Jpn. **74**, 30 (2005); source codes can be obtained from http://alps.comp-phys.org.
[35] S. K. Pati and C. N. R. Rao, J. Chem. Phys. **123**, 234703 (2005).